Cao et al. Bioresour. Bioprocess. (2017) 4:56
https://doi.org/10.1186/s40643-017-0186-0

Bioresources and Bioprocessing

RESEARCH Open Access

Magnetic ZIF-8/cellulose/Fe_3O_4 nanocomposite: preparation, characterization, and enzyme immobilization

Shi-Lin Cao[1,2†], Hong Xu[2,3,4†], Lin-Hao Lai[1], Wei-Ming Gu[1], Pei Xu[2,4], Jun Xiong[2], Hang Yin[2], Xue-Hui Li[3], Yong-Zheng Ma[5], Jian Zhou[3], Min-Hua Zong[2,3] and Wen-Yong Lou[2,4*]

Abstract

Background: The ZIF-8-coated magnetic regenerated cellulose-coated nanoparticles (ZIF-8@cellu@Fe_3O_4) were successfully prepared and characterized. The result showed that ZIF-8 was successfully composited on to the surface of the cellulose-coated Fe_3O_4 nanoparticles by co-precipitation method. Moreover, the glucose oxidase (GOx, from *Aspergillus niger*) was efficiently immobilized by the ZIF-8@Cellu@Fe_3O_4 nanocarriers with enhanced catalytic activities. The enzyme loading was 94.26 mg/g and the enzyme activity recovery was more than 124.2%. This efficiently immobilized enzyme exhibits promising applications in biotechnology, diagnosis, biosensing, and biomedical devices.

Conclusions: A new core–shell magnetic ZIF-8/cellulose nanocomposite (ZIF-8@Cellu@Fe_3O_4) was fabricated and structurally characterized. Glucose oxidase (GOx) was successfully immobilized by the biocompatible ZIF-8@Cellu@Fe_3O_4 with high protein loading (94.26 mg/g) and enhanced relative activity recovery (124.2%).

Keywords: Metal–organic frameworks, Glucose oxidase, Zeolitic imidazolate framework

Background

Metal–organic frameworks (MOFs) show attractive applications in various fields including gas adsorption (Li et al. 2009) and chemical separation (Maes et al. 2010), and catalysis (Lee et al. 2009). Zeolitic imidazolate framework (ZIF) materials belong to an important class of MOF (Phan et al. 2010), which exhibit the tunable pore size, chemical functionality of classical MOFs, exceptional chemical stability, and structural diversity of zeolites (Wu et al. 2007). Because of these features, ZIFs show great promise for enzyme immobilization (Hou et al. 2017; Wu et al. 2017). Hou et al. (2015) reported the construction of mimetic multi-enzyme systems by embedding GOx in ZIF-8 and application of this system as biosensors for glucose detection, exhibiting extraordinary electro-detection performance, and lower detection limit. Lyu et al. (2014) reported one-step immobilization process for protein-embedded metal–organic frameworks with enhanced activities, in which the Cyt c immobilized by ZIF-8 carrier exhibited an enhancement of enzyme activity compared with free Cyt c.

In order to separate the MOF-based materials easily, previous studies have reported on MOF-functionalized magnetic nanoparticles which can be recycled under magnetic field and have excellent physical and chemical characters of the MOF shell (Ke et al. 2012). Further investigations on magnetic MOFs with core–shell structure are still needed because the controllable growth of the MOF crystals on the magnetic nanoparticles remains a great challenge (Nong et al. 2015). For instance, before the MOF crystal growth process, the magnetic nanoparticles need to be surface-modificated by styrene sulfonate (Zhang et al. 2013), polyacrylic acid (Jin et al. 2014), chitosan (Xia et al. 2017), and SiO_2 (Wehner et al. 2016). It is worthy to note that cellulose may be acted as a promising

*Correspondence: wylou@scut.edu.cn
†Hong Xu and Shi-Lin Cao are both co-first author and contribute equally to this work.
[4] Guangdong Province Key Laboratory for Green Processing of Natural Products and Product Safety, South China University of Technology, No. 381 Wushan Road, Guangzhou 510640, China
Full list of author information is available at the end of the article

surface material, because of its abundance of hydroxyl groups. These hydroxyl groups may promote the adsorption of metal ions for the formation of MOF crystal (Liu et al. 2012). Cellulose is the most abundant renewable polysaccharide on earth, which is sustainable, biocompatible, biodegradable, and non-toxic (Lavoine et al. 2012). Previous studies showed that cellulose can dissolve in NaOH/urea aqueous media under − 12 °C, and surface modified the Fe_3O_4 magnetic nanoparticles (Cai and Zhang 2005). Thus, investigating the growth of the MOF onto the cellulose-modified Fe_3O_4 is of interest.

The glucose oxidase (GOx) is an aerobic dehydrogenation enzyme, which has played an important role on deoxidization, glucose removal, and gluconic acid synthesis. It is widely used in forage, medicine, and other fields (Wong et al. 2008). In recent years, in order to overcome the disadvantages of the free GOx such as poor mechanical stability, difficult separation, and non-recyclability (Cao et al. 2016), several nanoparticles, such as titanium dioxide nanotubes (Ravariu et al. 2011), Fe_3O_4/APTES (França 2014), Ag@Zn-TSA (Dong et al. 2016), and ZIF-8 (Wu et al. 2015) were attempted to be used as enzyme carriers for the immobilization of GOx. Among these nanoparticles, carriers containing metal–organic frameworks (MOFs) have received more and more concern because of their excellent physical and chemical properties mentioned above.

In this study, a new core–shell magnetic ZIF-8-coated magnetic regenerated cellulose-coated nanoparticle (ZIF-8@Cellu@Fe_3O_4) was fabricated. The as-prepared ZIF-8@Cellu@Fe_3O_4 was structurally characterized in detail. The glucose oxidase (GOx) was embedded in the pores of the ZIF-8@Cellu@Fe_3O_4 with a high relative activity recovery and protein loading.

Methods

Preparation of magnetic regenerated cellulose-coated nanoparticle (Cellu@Fe_3O_4)

The Fe_3O_4 nanoparticles were fabricated by co-precipitation method according to our previous literatures (Deng et al. 2016; Cao et al. 2017): 2.43 g $FeCl_3{\cdot}6H_2O$ and 0.9 g $FeCl_2{\cdot}4H_2O$ were dissolved in 200 mL deionized water at room temperature. The mixture was added dropwise into a 25% ammonia solution with stirring, N_2 purge, and the pH at 10. The temperature was raised to 60 °C and kept for 1 h; the magnetite precipitate was collected with an external magnet and washed three times with deionized water.

150 mg of Fe_3O_4 was dispersed in 30 mL aqueous solution containing 7 wt% of NaOH and 12 wt% of urea and pre-cooled to − 12 °C for more than 1 h. Then, 100 mg of microcrystalline cellulose was added into the above suspension. After 1 h of freezing, the microcrystalline cellulose was dissolved completely. Then the deionized water was mixed with the above mixture and the cellulose-coated Fe_3O_4 (Cellu@Fe_3O_4) was formed. The Cellu@Fe_3O_4 was collected with an external magnet and washed three times with deionized water.

Preparation of magnetic ZIF-8 nanoparticles (ZIF-8@Cellu@Fe_3O_4)

Zinc nitrate hexahydrate was dissolved in deionized water (40 mM, 2 mL) mixed with 10 mg Cellu@Fe_3O_4 under stirring for 20 min. Then 2-methylimidazole (160 mM, 2 mL) was added into the mixture and stirred for 3 h (Liang et al. 2015).

Preparation of GOx-loaded ZIF-8@Cellu@Fe_3O_4 nanocomposite

The synthesis processes of GOx-loaded ZIF-8@Cellu@Fe_3O_4 nanocomposites are illustrated in Scheme 1. Zinc nitrate hexahydrate was dissolved in deionized water (40 mM, 2 mL) mixture and stirring with 10 mg of Cellu@Fe_3O_4 for 20 min. Then 2-methylimidazole (160 mM, 2 mL) was added into the mixture and stirred for 10 min (Lyu et al. 2014; Liang et al. 2015; Du et al. 2017). Free GOx was dissolved in buffer (200 mM, pH 4.0–8.0); 0.2 mL free enzyme (100 U/mL) was added into solutions. The reaction lasted for (0.5–3 h) and immobilized at (10–50 °C, 200 rpm). The immobilized GOx was separated through an external magnetic field. Then, the un-immobilized GOx was removed by continuous washing until no protein was detected. The washing solutions were collected to detect the amount of un-immobilized GOx. The amount of immobilized GOx loaded on the ZIF-8@Cellu@Fe_3O_4 was calculated as the difference between the initial and the un-immobilized GOx. The GOx-loaded ZIF-8@Cellu@Fe_3O_4 was named as GOx-ZIF-8@Cellu@Fe_3O_4.

Enzyme activity assay and protein concentration

Protein concentration was determined according to the Bradford method using bovine serum albumin as standard (Lowry et al. 1951).

The activities of free and immobilized glucose oxidase were determined by indigo carmine method (Zhou et al. 2008). Glucose oxidase was dissolved in 1 mL phosphate buffer (200 mM, pH 7.0) and then 4 mL 0.2 mol/L glucose solution was added. The solution was mixed at 37 °C for 10 min. 3 mL acetic acid–sodium acetate (0.1 M acetic acid 500 mL and 0.1 M sodium acetate 30 mL, pH 3.5) was added as buffer solution, and 1.3 mL indigo carmine (0.1 mM) was used as redox indicator. After treated at 100 °C (boiling water) for 13 min, the absorbance of solution at wavelength of 615 nm was measured.

Activity recovery (%) was calculated as follows:

$$= 100 \times \frac{\text{Activity of immobilized enzyme (U)}}{\text{Activity of free enzyme used for immobilization (U)}}.$$

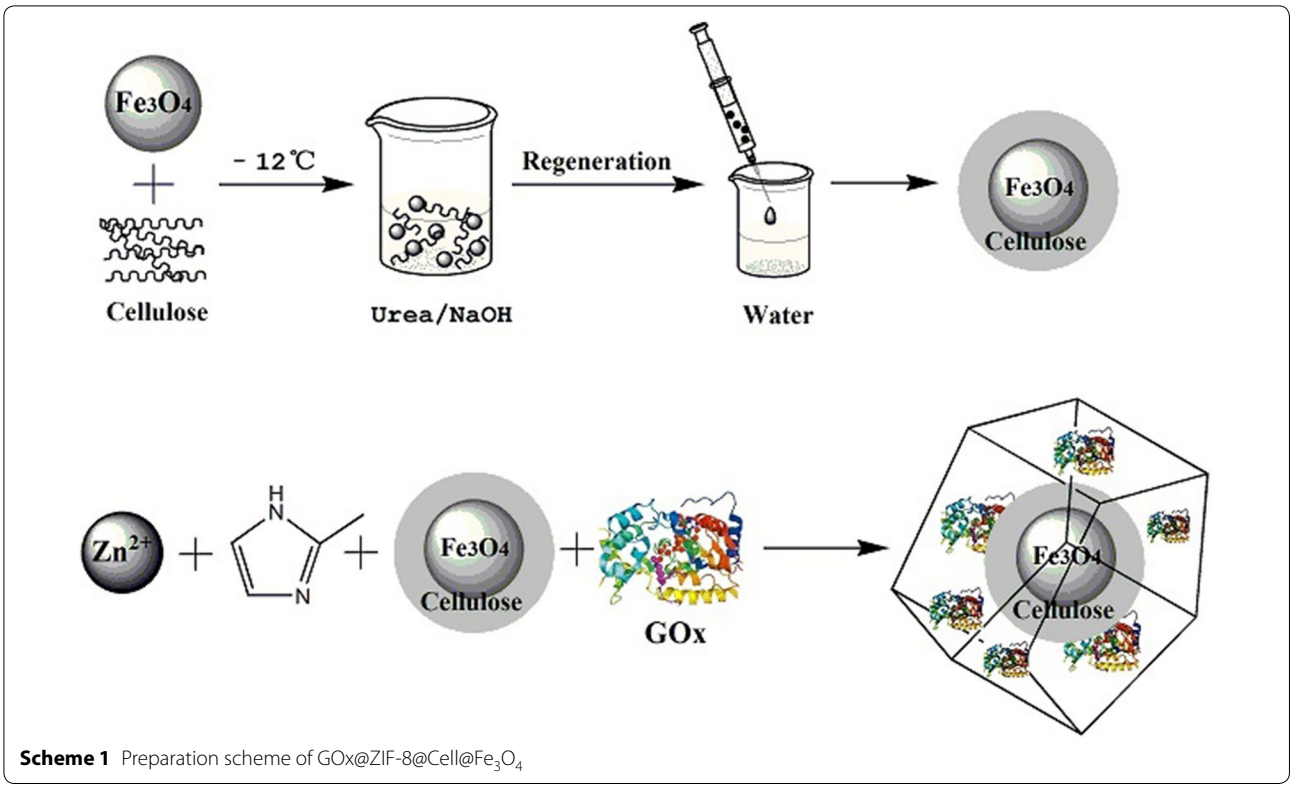

Scheme 1 Preparation scheme of GOx@ZIF-8@Cell@Fe_3O_4

Enzyme loading (%) was calculated as follows:

$$= 100 \times \frac{\text{Enzyme content of immobilized enzyme (mg)}}{\text{Content of enzyme used for immobilization (mg)}}.$$

Results and discussion

Characterization of Cellu@Fe_3O_4 and ZIF-8@Cellu@Fe_3O_4

The X-ray diffraction patterns of the ZIF-8@Cellu@Fe_3O_4, Cellu@Fe_3O_4, microcrystalline cellulose, and naked Fe_3O_4 are shown in Fig. 1. However, the microcrystalline cellulose showed three peaks at $2\theta = 14.8°$, 16.5°, and 22.7° assigned to the (110), (110), and (200) planes which were characteristic peaks for the cellulose crystalline (I) (Edwards et al. 2012). By comparison, the Cellu@Fe_3O_4 displayed three diffraction peaks at $2\theta = 12.4°$, 20.2°, and 22.2° assigned to the (110), (110), and (200) planes of cellulose crystalline (II) (Togawa and Kondo 1999). This illustrated that after dissolving-regeneration process, the cellulose crystalline form changed from cellulose (I) to cellulose (II) (Carrillo et al. 2004). Moreover, the Cellu@Fe_3O_4 showed four distinct peaks at $2\theta = 30.24°$, 35.60°, 43.24°, and 57.16°, ascribing to the crystal plane diffraction peaks of the (220), (400), (422), and (511) diffraction peaks for Fe_3O_4 (JCPDS Card No. 19–0629) (Cao et al. 2014). The ZIF-8@Cellu@Fe_3O_4 XRD pattern is also shown in Fig. 1. The result showed that visible diffraction peaks at about $2\theta = 7.3°$, 10.5°, and 18.0° were assigned to the characteristic diffraction peak of ZIF-8 (Pan et al. 2011). These results indicated the formation of the ZIF-8@Cellu@Fe_3O_4.

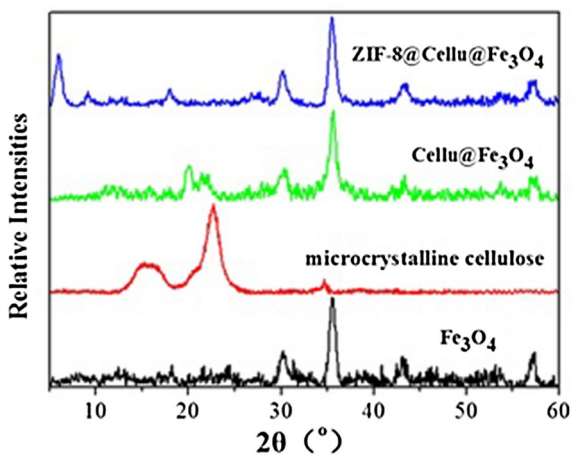

Fig. 1 The powder X-ray diffraction patterns of ZIF-8@Cellu@Fe_3O_4, Cellu@Fe_3O_4, and microcrystalline cellulose

Figure 2 shows the FTIR spectra of ZIF-8@Cellu@Fe_3O_4, Cellu@Fe_3O_4, and microcrystalline cellulose. For the microcrystalline cellulose (Fig. 2a), the band at 1431 cm^{-1} was attributed to C–O–H stretching vibration. However, for Cellu@Fe_3O_4 (Fig. 2b), the peak at 1431 cm^{-1} disappeared and peak at 1421 cm^{-1} was observed (Colom and Carrillo 2002). This also illustrated

that after dissolving-regeneration process, the cellulose crystalline form of Cellu@Fe_3O_4 changed from cellulose (I) to cellulose (II) (Colom and Carrillo 2002). Moreover, there was a strong absorption peak of Cellu@Fe_3O_4 at around 594 cm^{-1} assigned to the characteristic peak of Fe_3O_4 (Cornell et al. 1999). Also, the bands of Cellu@Fe_3O_4 at 3440 cm^{-1}, attributed to hydrogen bonding of cellulose, became broader and weaker, illustrating the strong interaction between Fe_3O_4 and cellulose layer which were observed (Kondo et al. 1994; Kondo and Sawatari 1996; Zhang et al. 2001). The FTIR spectrum shown in Fig. 2c displays the chemical composition of the ZIF-8@Cellu@Fe_3O_4. A strong peak at 421 cm^{-1} is ascribed to the Zn–N stretch mode (Zhang et al. 2013). The broad bands around 500–1350 and 1350–1500 cm^{-1} were assigned as the plane bending and stretching of imidazole ring, respectively (Lu et al. 2012). These results showed that the ZIF-8 was successfully composited on to the surface of the Cellu@Fe_3O_4 by co-precipitation method.

As shown in the scanning electron microscope (SEM) graphy (Fig. 3), the Cellu@Fe_3O_4 has an average diameter of around 29.7 nm and displays uniform structure and morphology. The size of ZIF-8@Cellu@Fe_3O_4 was approximated to 170 nm.

The vibrating specimen magnetometer (VSM) magnetization curves of the Cellu@Fe_3O_4 and ZIF-8@Cellu@Fe_3O_4 are shown in Fig. 4. Saturation magnetization (M_S) was used to measure the magnetization of samples defined as the maximum magnetic response of a material in an external magnetic field (Xiao et al. 2014). It is observed that the M_S of Fe_3O_4 is 21.37 emu/g and of ZIF-8@Cellu@Fe_3O_4 (4.9 emu/g) is lower than that of Cellu@Fe_3O_4 nanoparticles (12.8 emu/g).

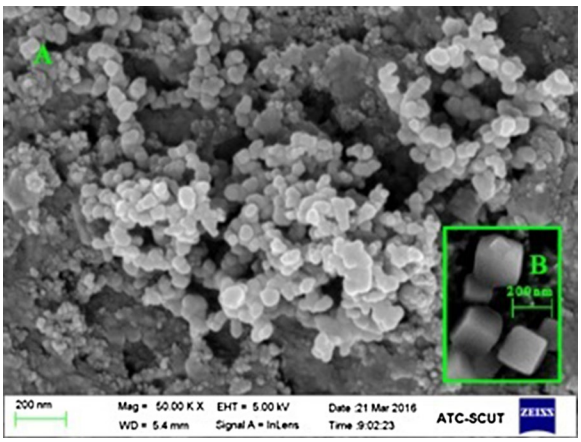

Fig. 3 SEM graphy of Cellu@Fe_3O_4 (**A**), ZIF-8@Cellu@Fe_3O_4 (**B**)

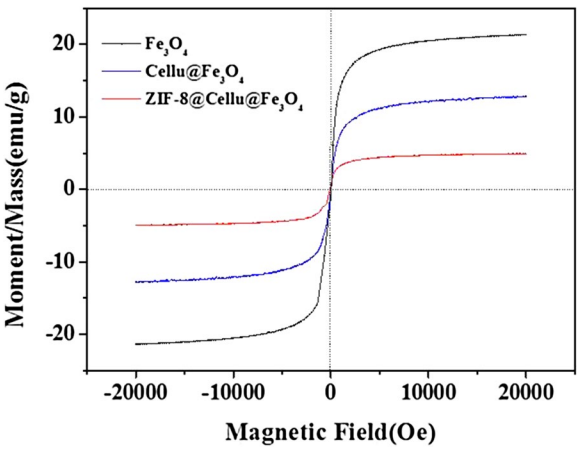

Fig. 4 Hysteresis loops of Fe_3O_4, Cellu@Fe_3O_4, ZIF-8@Cellu@Fe_3O_4, and GOx-ZIF-8@Cellu@Fe_3O_4

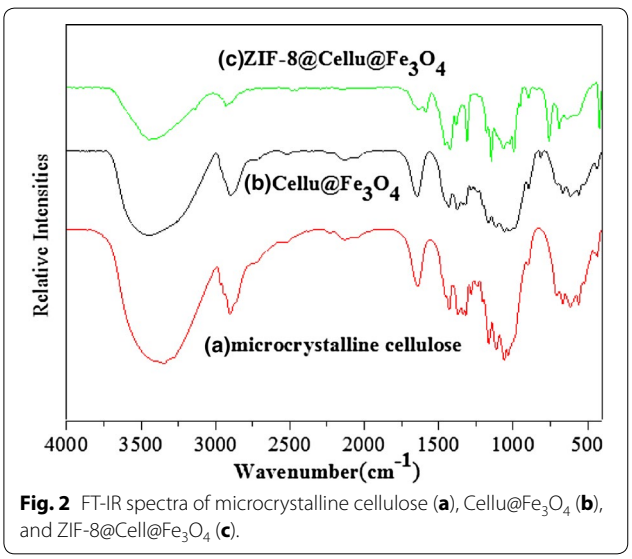

Fig. 2 FT-IR spectra of microcrystalline cellulose (**a**), Cellu@Fe_3O_4 (**b**), and ZIF-8@Cell@Fe_3O_4 (**c**).

Immobilization of GOx by ZIF-8@Cellu@Fe_3O_4 nanocomposite

Figure 5 shows the effect of buffer pH on enzyme activity recovery and enzyme loading. The results show that the highest activity recovery of immobilized glucose oxidase (GOx-ZIF-8@Cellu@Fe_3O_4) displayed at pH 7.0 (123.7%), with the protein loading 91.3 mg/g. The GOx-ZIF-8@Cellu@Fe_3O_4 exhibited relative high activity at faintly acid and neutral conditions (pH 6.5–7.0), and became deactivated in the both the acid and alkaline conditions (Cao et al. 2008). Also, ZIF-8 is very stable in neutral and basic conditions (Jian et al. 2015) and exhibit best enzyme encapsulation capacity at pH 7.5–8.0. Thus, the protein loading capacity changed depending on different pH values and the optimal pH value for GOx immobilization was 7.0.

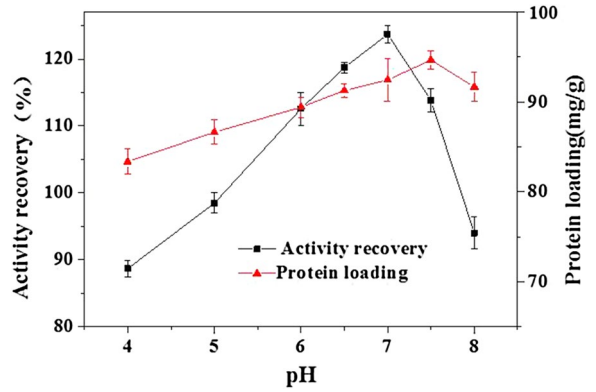

Fig. 5 Effects of buffer pH on activity recovery and enzyme loading of immobilized GOx

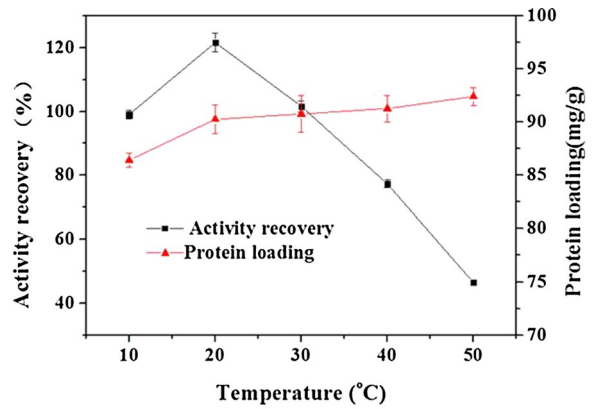

Fig. 6 Effects of immobilization temperature on activity recovery and enzyme loading of immobilized GOx

Figure 6 shows the effect of immobilization temperature on activity recovery and enzyme loading. The results showed that the GOx-ZIF-8@Cellu@Fe_3O_4 with highest activity recovery was obtained at 20 °C. When the temperature was higher than 30 °C, enzyme activity recovery decreased significantly. Thus, 20 °C was selected as the immobilization temperature in the following experiment.

Figure 7 shows the effect of immobilization time on enzyme activity recovery and enzyme loading. The result shows that when the immobilization time was 1 h, the highest relative activity was obtained. After 1 h, the relative activity decreased gradually, which was possibly due to the partial inactivation of the enzyme with immobilized time prolonged. In conclusion, the optimum immobilization time was 1 h at which the activity recovery of GOx attained 124.2% and the enzyme loading was 94.26 mg/g.

Generally speaking, the optimal condition of the immobilization process was that buffer pH 7, temperature 20 °C, and immobilization time 1 h. At this condition, the activity recovery was 124.2%, and the enzyme loading was

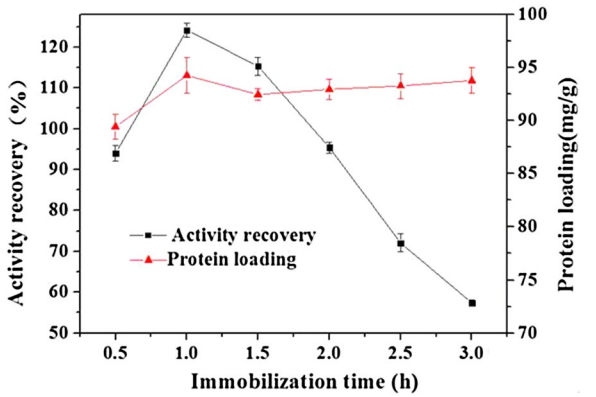

Fig. 7 Effects of immobilization time on activity recovery and enzyme loading of immobilized GOx

94.26 mg/g. The specific enzyme activity values of immobilized and free GOx were 12.42 and 10.00 U/mg, respectively. The thermal stability of free and immobilized GOx at 65 °C was performed. The activities of both free and immobilized GOx decreased gradually with increasing of the incubation time. The immobilized GOx exhibited more than 40% of its initial activity after 4 h of incubation, while that of free GOx was about 13%. This result showed that the thermal stability of immobilized GOx was enhanced after immobilization (Zhou et al. 2012a, b). As a comparison, GOx immobilized onto a 3-(aminopropyl)triethoxysilane (APTES)-coated Fe_3O_4 nanocarrier which retained less than 50% of the native GOx activity (Park et al. 2011). Thus the immobilization process in the present study is promising for enzyme immobilization.

A comparative study shown in Fig. 8 explores the mechanism of the enhanced enzyme relatively activity after immobilization. The presence of Cellu@Fe_3O_4,

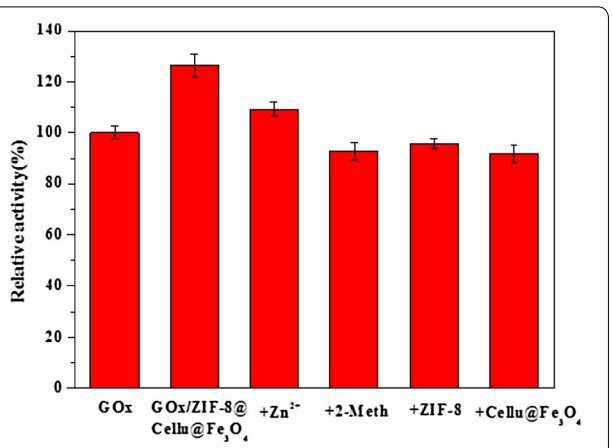

Fig. 8 The relative peroxidase activity of GOx, GOx-ZIF-8@Cellu@Fe_3O_4 composite, GOx/zinc ion mixture, GOx/2-methylimidazole mixture, GOx/ZIF-8 mixture, and GOx/Cellu@Fe_3O_4 mixture

ZIF-8 and 2-methylimidazole could not enhance the activity of GOx, while that of Zn^{2+} increased the activity of GOx by about 9.3%, which was similar with the previous literature (Lyu et al. 2014). Comparison shows that the immobilization of GOx in ZIF-8@Cellu@Fe_3O_4 enhanced the activity of GOx by 24.2%. These results showed that the GOx-ZIF-8@Cellu@Fe_3O_4 exhibited an increased relative activity compared to the free GOx. This may be attributed to the following reason: the enzyme immobilization process changed the enzyme conformation and increased the substrate affinity toward the glucose; the interaction between the GOx and Zn^{2+} in ZIF-8 enhanced the catalytic activity (Lyu et al. 2014).

Conclusions

In conclusion, Glucose oxidase (GOx) was successfully immobilized onto the biocompatible ZIF-8@Cellu@Fe_3O_4 via co-precipitation process. Its morphology, structure, and magnetic properties were determined. The GOx immobilized in ZIF-8@Cellu@Fe_3O_4 had high protein loading (94.26 mg/g) and enhanced relative activity recovery (124.2%). The results of the present work provide an efficient enzyme immobilization process and promote the application and development of immobilized enzyme catalysis.

Abbreviations

GOx: glucose oxidase; MOFs: metal–organic frameworks; ZIF: zeolitic imidazolate framework; Cellu@Fe_3O_4: magnetic regenerated cellulose-coated nanoparticle; ZIF-8@Cellu@Fe_3O_4: ZIF-8-coated magnetic regenerated cellulose nanoparticle; GOx-ZIF-8@Cellu@Fe_3O_4: GOx-loaded ZIF-8@Cellu@Fe_3O_4 nanocomposite.

Authors' contributions

Conceived and designed the experiments: SLC, XH, WYL, and MHZ. Performed the experiments: SLC, XH, WMG, and LHL. Analyzed the data: XH, SLC, XP, JX, HY, and YZM. Contributed reagents/materials/analysis tools: MHZ, WYL, and JZ. Wrote the paper: XH, SLC, YZM, and WYL. All authors read and approved the final manuscript.

Author details

[1] Department of Food Science, Foshan University (Northern Campus), Nanhai, Foshan 528231, China. [2] Laboratory of Applied Biocatalysis, School of Food Science and Engineering, South China University of Technology, No.381 Wushan Road, Guangzhou 510640, China. [3] School of Chemistry and Chemical Engineering, South China University of Technology, No. 381 Wushan Road, Guangzhou 510640, China. [4] Guangdong Province Key Laboratory for Green Processing of Natural Products and Product Safety, South China University of Technology, No. 381 Wushan Road, Guangzhou 510640, China. [5] School of Marine Science and Technology, Tianjin University, 92 Weijin Road, Tianjin 300072, China.

Acknowledgements

Not applicable.

Competing interests

The authors declare that they have no competing interests.

Availability of data and materials

All data generated or analyzed during this study are included in this article.

Consent for publication

All authors have read and approved to submit it to Bioresources and Bioprocessing. There is no conflict of interest of any author in relation to the submission.

Ethics approval and consent to participate

Not applicable.

Funding

The National Natural Science Foundation of China (21336002; 21676104; 21376096), the Fundamental Research Funds for the Chinese Universities (2015PT002; 2015ZP009), the Program of State Key Laboratory of Pulp and Paper Engineering (2017ZD05), the Open Funding Project of the State Key Laboratory of Bioreactor Engineering, and High-Level Talent Start-Up Research Project of Foshan University (GG07016).

Publisher's Note

Received: 26 September 2017 Accepted: 18 December 2017
Published online: 26 December 2017

References

Cai J, Zhang L (2005) Rapid dissolution of cellulose in LiOH/urea and NaOH/urea aqueous solutions. Macromol Biosci 5:539

Cao L, Ye J, Tong L et al (2008) A new route to the considerable enhancement of glucose oxidase (GOx) activity: the simple assembly of a complex from CdTe quantum dots and GOx, and its glucose sensing. Chemistry 14:9633–9640

Cao S-L, Li X-H, Lou W-Y et al (2014) Preparation of a novel magnetic cellulose nanocrystal and its efficient use for enzyme immobilization. J Mater Chem B 2:5522–5530

Cao S, Xu P, Ma Y et al (2016) Recent advances in immobilized enzymes on nanocarriers. Chin J Catal 37:1814–1823

Cao S-L, Deng X, Xu P et al (2017) Highly efficient enzymatic acylation of dihydromyricetin by the immobilized lipase with deep eutectic solvents as co-solvent. J Agric Food Chem 65:2084–2088

Carrillo F, Colom X, Suñol JJ et al (2004) Structural FTIR analysis and thermal characterisation of lyocell and viscose-type fibres. Eur Polym J 40:2229–2234

Colom X, Carrillo F (2002) Crystallinity changes in lyocell and viscose-type fibres by caustic treatment. Eur Polym J 38:2225–2230

Cornell RM, Schwertmann U, Cornell R (1999) The iron oxides: structure, properties, reactions, occurrences and uses. Clay Miner 34:209–210

Deng X, Cao S, Li N et al (2016) A magnetic biocatalyst based on mussel-inspired polydopamine and its acylation of dihydromyricetin. Chin J Catal 37:584–595

Dong S, Zhang D, Suo G et al (2016) Exploiting multi-function metal–organic framework nanocomposite Ag@Zn-TSA as highly efficient immobilization matrixes for sensitive electrochemical biosensing. Anal Chim Acta 934:203–211

Du Y, Gao J, Zhou L et al (2017) Enzyme nanocapsules armored by metal–organic frameworks: a novel approach for preparing nanobiocatalyst. Chem Eng J 327:1192–1197

Edwards JV, Prevost NT, Condon B et al (2012) Immobilization of lysozyme–cellulose amide-linked conjugates on cellulose I and II cotton nanocrystalline preparations. Cellulose 19:495–506

França TCP (2014) Preparation and characterization of hybrid Fe3O4/APTES for immobilization of GOX. Mater Sci Forum 798–799:460–465

Hou C, Wang Y, Ding Q et al (2015) Facile synthesis of enzyme-embedded magnetic metal–organic frameworks as a reusable mimic multi-enzyme system: mimetic peroxidase properties and colorimetric sensor. Nanoscale 7:18770

Hou M, Zhao H, Feng Y et al (2017) Synthesis of patterned enzyme–metal–organic framework composites by ink-jet printing. Bioresour Bioprocess 4:40

Jian M, Liu B, Zhang G et al (2015) Adsorptive removal of arsenic from aqueous solution by zeolitic imidazolate framework-8 (ZIF-8) nanoparticles. Colloids Surf A Physicochem Eng Aspects 465:67–76
Jin T, Yang Q, Meng C et al (2014) Promoting desulfurization capacity and separation efficiency simultaneously by the novel magnetic Fe3O4@PAA@MOF-199. RSC Adv 4:41902–41909
Ke F, Qiu LG, Yuan YP et al (2012) Fe3O4@MOF core–shell magnetic microspheres with a designable metal–organic framework shell. J Mater Chem 22:9497–9500
Kondo T, Sawatari C (1996) A Fourier transform infra-red spectroscopic analysis of the character of hydrogen bonds in amorphous cellulose. Polymer 37:393–399
Kondo T, Sawatari C, Manley RSJ et al (1994) Characterization of hydrogen bonding in cellulose-synthetic polymer blend systems with regioselectively substituted methylcellulose. Macromolecules 27:210–215
Lavoine N, Desloges I, Dufresne A et al (2012) Microfibrillated cellulose—its barrier properties and applications in cellulosic materials: a review. Carbohydr Polym 90:735
Lee J, Farha OK, Roberts J et al (2009) Metal–organic framework materials as catalysts. Chem Soc Rev 38:1450–1459
Li J-R, Kuppler RJ, Zhou H-C (2009) Selective gas adsorption and separation in metal–organic frameworks. Chem Soc Rev 38:1477–1504
Liang K, Ricco R, Doherty CM et al (2015) Biomimetic mineralization of metal–organic frameworks as protective coatings for biomacromolecules. Nat Commun 6:7240
Liu Z, Wang H, Liu C et al (2012) Magnetic cellulose–chitosan hydrogels prepared from ionic liquids as reusable adsorbent for removal of heavy metal ions. Chem Commun 48:7350
Lowry OHNG, Rosebrough NJJ, Farr AL et al (1951) Protein measurement with folin phenol reagent. J Biol Chem 193:265–275
Lu G, Li S, Guo Z et al (2012) Imparting functionality to a metal–organic framework material by controlled nanoparticle encapsulation. Nat Chem 4:310
Lyu F, Zhang Y, Zare RN et al (2014) One-pot synthesis of protein-embedded metal–organic frameworks with enhanced biological activities. Nano Lett 14:5761
Maes M, Alaerts L, Vermoortele F et al (2010) Separation of C(5)-hydrocarbons on microporous materials: complementary performance of MOFs and zeolites. J Am Chem Soc 132:2284–2292
Nong J, Zhao W, Qin X et al (2015) Recent progress in the study of core–shell-structured materials with metal organic frameworks (MOFs) as shell. Chem Ind Eng Prog 34:774–783
Pan Y, Liu Y, Zeng G et al (2011) Rapid synthesis of zeolitic imidazolate framework-8 (ZIF-8) nanocrystals in an aqueous system. Chem Commun 47:2071–2073
Park HJ, McConnell JT, Boddohi S et al (2011) Synthesis and characterization of enzyme–magnetic nanoparticle complexes: effect of size on activity and recovery. Colloids Surf B Biointerfaces 83:198–203
Phan A, Doonan CJ, Uriberomo FJ et al (2010) Synthesis, structure, and carbon dioxide capture properties of zeolitic imidazolate frameworks. Acc Chem Res 43:58–67
Ravariu, Manea, Parvulescu et al (2011) Titanium dioxide nanotubes on silicon wafer designated for GOX enzymes immobilization. Dig J Nanomater Biostruct 6:703–707
Togawa E, Kondo T (1999) Change of morphological properties in drawing water-swollen cellulose films prepared from organic solutions. A view of molecular orientation in the drawing process. J Polym Sci, Part B: Polym Phys 37:451–459
Wehner T, Mandel K, Schneider M et al (2016) Superparamagnetic luminescent MOF@Fe_3O_4/SiO_2 composite particles for signal augmentation by magnetic harvesting as potential water detectors. ACS Appl Mater Interfaces 8:5445
Wong CM, Wong KH, Chen XD (2008) Glucose oxidase: natural occurrence, function, properties and industrial applications. Appl Microbiol Biotechnol 78:927–938
Wu H, Zhou W, Yildirim T (2007) Hydrogen storage in a prototypical zeolitic imidazolate framework-8. J Am Chem Soc 129:5314
Wu X, Ge J, Yang C et al (2015) Facile synthesis of multiple enzyme-containing metal–organic frameworks in a biomolecule-friendly environment. Chem Commun 51:13408
Wu X, Yang C, Ge J (2017) Green synthesis of enzyme/metal–organic framework composites with high stability in protein denaturing solvents. Bioresour Bioprocess 4:24
Xia GH, Cao SL, Xu P et al (2017) Preparation of a nanobiocatalyst by efficiently immobilizing *Aspergillus niger* lipase onto magnetic metal–biomolecule frameworks (BioMOF). ChemCatChem 9:1794–1800
Xiao F, Feng C, Jin C et al (2014) Magnetic and electromagnetic properties of Fe_3O_4/C self-assemblies. Mater Lett 122:103–105
Zhang L, Ruan D, Zhou J (2001) Structure and properties of regenerated cellulose films prepared from cotton linters in NaOH/urea aqueous solution. Ind Eng Chem Res 40:5923–5928
Zhang T, Zhang X, Yan X et al (2013) Synthesis of Fe3O4@ZIF-8 magnetic core–shell microspheres and their potential application in a capillary microreactor. Chem Eng J 228:398–404
Zhou JQ, Chen SH, Wang JW (2008) A simple and convenient method to determine the activity of glucose oxidase. Exp Technol Manag 12:15
Zhou L, Jiang Y, Gao J et al (2012a) Oriented immobilization of glucose oxidase on graphene oxide. Biochem Eng J 69:28–31
Zhou L, Jiang Y, Gao J et al (2012b) Graphene oxide as a matrix for the immobilization of glucose oxidase. Appl Biochem Biotechnol 168:1635–1642